Nanomechanical Cantilever Motion Generated by a Surface-Confined Redox Reaction

Florence Quist, Vincent Tabard-Cossa,† and Antonella Badia*

Department of Chemistry, Université de Montréal, C.P. 6128, succursale Centre-ville, Montréal, QC H3C 3J7 Canada

Received: June 5, 2003; In Final Form: August 10, 2003

Interfacial stress changes at electroactive self-assembled monolayers have been investigated by monitoring the potential-induced deflection of Au-coated microcantilevers modified with 12-ferrocenyl-1-dodecanethiol in aqueous perchloric acid solution. Oxidation of the surface-bound ferrocene generates a compressive surface stress which results in the cantilever bending away from the film-coated Au surface. The origin of the redox-induced stress change that occurs at these close-packed monomolecular films is discussed.

Introduction

We demonstrate herein using a microcantilever sensor[1−6] that the introduction of charges at an electroactive self-assembled monolayer (SAM)/solution interface via a redox reaction can be transduced into a mechanical motion. The cantilever sensor bends in response to surface stress changes generated by contracting (tensile) or expanding (compressive) interactions between molecules bound to the surface of one face of the lever. This work was motivated by recent experiments that demonstrate that microfabricated cantilevers modified with carboxylic acid- or amine-terminated SAMs can be induced to bend by deprotonation/protonation of the ionisable acid/base groups.[4,7−9] In the past decade, much use has been made of self-assembled alkanethiolate monolayer films to tailor the interfacial properties of coinage metal surfaces for a variety of applications (chemical and biological sensing, corrosion, molecular electronics, adhesion, lithography).[10−12] In addition to serving as model systems for the investigation of long-range electron transfer,[13,14] SAM-tethered redox species have enabled researchers to electrochemically modulate surface interactions through potential-induced changes in adhesion[15,16] and wetting[17,18] properties. Electroactive SAMs have, for example, been used to control liquid flow down an inclined surface,[17] guide the orthogonal assembly of charged nanostructures,[19] manipulate and position objects with an atomic force microscopy (AFM) tip,[20] and selectively release or immobilize biologically active ligands.[21,22]

To date, underpotential metal deposition,[23,24] electrocapillary effects,[24,25] and doping/dedoping of a thick, conducting polymer film coating[26] have been used to electrochemically drive the nanomechanical response of metal-coated cantilevers. We report that the electrochemical transformation of a redox moiety (ferrocene) in a *monomolecular* organic film can generate a surface stress change of sufficient magnitude to deflect a microcantilever (Scheme 1). The electrogeneration of ferrocenium cations and their association with counterions are confined to the ferrocenylalkanethiolate monolayer/solution interface.[27] This feature renders electroactive SAMs a potentially interesting system to investigate the dependence of the voltage-induced micromechanical motion on the concentration of the redox moieties in the SAM and on their distance from the cantilever surface.

SCHEME 1: Schematic Representation of the Potential-Induced Deflection of a $FcC_{12}S$−Au Cantilever

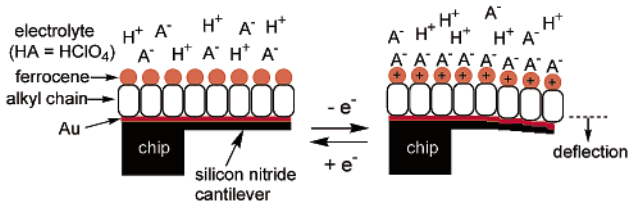

Experimental Section

12-Ferrocenyl-1-dodecanethiol ($FcC_{12}SH$) was synthesized and purified according to the procedure of Creager and Rowe.[28] Friedel−Crafts acylation of ferrocene with 12-bromododecanoyl chloride (in CH_2Cl_2 with $AlCl_3$), Clemmenson reduction of the resulting 12-(ferrocenylcarbonyl)undecyl bromide with a zinc−mercury amalgam (in toluene−aqueous 12 M HCl), and conversion of the bromide to the thiol by reaction with sodium thiosulfate followed by acid hydrolysis of the Bunte salt afforded the desired $FcC_{12}SH$. The identity and purity of the product was verified by thin-layer chromatography and ^1H NMR spectroscopy.

Standard V-shaped silicon nitride cantilevers (0.6 μm thickness, 193 μm length, 36 μm wide, 0.12 N/m spring constant, surface area of each face $\approx 1.6 \times 10^{-4}$ cm^2) were purchased from Digital Instruments/Veeco. The reflective Au coating was first removed from the cantilever chips using dilute aqua regia (3:1:6 $HCl:HNO_3:H_2O$), and the tip-containing side of the cantilever chips was then coated with 5 nm of Ti (adhesion layer) and 85 nm of Au by thermal evaporation. Au surfaces for ellipsometry measurements were prepared by depositing ∼5 nm of Ti followed by ∼45 nm of Au on glass microscope slides (Fisherbrand). Following metal deposition, the Au-coated cantilevers and slides were immersed in a 1 mM solution of either $FcC_{12}SH$ or decanethiol ($C_{10}SH$, 96%, Sigma-Aldrich) in 4:1 ethanol/THF for ∼18 h. Previous studies by Whitesides and co-workers have demonstrated the selective chemisorption (>100:1) of *n*-alkanethiols and ferrocene-terminated alkanethiols to Au compared to their physisorption to silicon nitride.[29,30] Upon removal from the incubation solution, the modified cantilevers and slides were rinsed with absolute ethanol and dried under a stream of nitrogen.

A homemade, optical beam deflection setup was combined with a BAS 100B/W potentiostat (Bioanalytical Systems) to

* Corresponding author. E-mail: antonella.badia@umontreal.ca.
† Presently at McGill University (Montréal, QC), Department of Physics.

10.1021/jp0355915 CCC: $25.00
Published on Web 09/06/2003

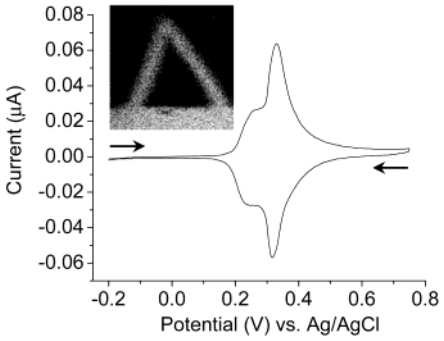

Figure 1. Cyclic voltammogram of a $FcC_{12}SH$-modified Au cantilever substrate in 1.0 M $HClO_4$. Scan rate = 5 mV/s. The arrows indicate the direction of potential cycling. Inset: spatially resolved TOF−SIMS ion map of Fe^+ (*m*/*z* ratio of 56 amu) on a $FcC_{12}SH$-modified Au-coated cantilever. The distribution of Fe^+ across the 193 μm long cantilever and part of the chip surface is shown. Lighter areas correspond to higher Fe^+ ion intensity. Image size = 252 μm × 252 μm.

monitor the static deflection of a $FcC_{12}SH$-modified cantilever as a function of the applied potential during a cyclic voltammetry experiment. The Au-coated rectangular cantilever chip (1.7 mm × 3.6 mm) serves as the working electrode in an electrochemical liquid cell (Figure 1S), which also contains a platinum wire counter electrode and a Ag/AgCl reference electrode (3 M NaCl, Bioanalytical Systems). A stainless steel clip holds the cantilever in place in the liquid cell and makes electrical contact to the Au-coated face. The chip is immersed into a 1.0 M $HClO_4$(aq) electrolyte solution to a depth of 1−2 mm using a precision micropositioner (Newport). The focused laser beam of a diode laser module (λ = 635 nm) is then positioned onto the apex of the cantilever immersed in the $HClO_4$ solution. The reflected beam is detected by a one-dimensional position sensing detector (PSD IL10, ON-TRAK Photonics, Inc.). The photocurrents generated at the PSD electrodes by the impinging light spot are sent to a transimpedance amplifier (current-to-voltage converter). The amplified photocurrent voltages are processed by an analog dividing chip to produce an ouput voltage that is independent of the laser intensity. This output voltage, which corresponds to the position of the light spot on the PSD, is then digitized using a 16-bit analog-to-digital converter card (PCI-MIO-16XE-10, National Instruments) and stored onto a PC using a data acquisition program written in LabView 5.1 (National Instruments). For the nanometer-scale deflections typically induced by surface stress phenomena at monolayer film interfaces,[7,31−37] the displacement of the impinging laser spot on the PSD is linearly proportional to the cantilever deflection, which is in turn directly proportional to the induced surface stress variation.[38,39] Because we are presently interested in relative (rather than absolute) changes, the cantilever deflection is expressed as the measured PSD voltage. Cantilever deflections that result in a decrease of the PSD voltage correspond to bending of the lever away from the Au-coated face. To rule out a contribution to the measured PSD signal from potential-induced changes in the reflectivity of the monolayer-coated Au surface, the laser was focused on the surface of a $FcC_{12}SH$-modified Au substrate. No significant change in the PSD signal was observed during potential cycling in this case.

Null ellipsometry was performed at a wavelength of 632.8 nm and incident angle of 70° on a Multiskop ellipsometer (Optrel GbR). A refractive index (*n*) value of 1.464 and an extinction coefficient (*k*) of 0.0741 were used for the $FcC_{12}S$−Au monolayer.[40] Time-of-flight static secondary-ion mass spectrometry (TOF−SIMS) analysis of unmodified and thiol-modified Au-coated cantilevers was performed with a TOF−SIMS IV instrument (Cameca/ION-TOF). Spatially resolved Fe^+ ion images were obtained in positive ion mode using Ga^+ as the primary ion with kinetic energy of 15 keV, a current of 0.83 pA and a pulse width of 28 ns. Au^+ ion images were obtained in negative ion mode with a current of 1.17 pA and a pulse width of 28 ns. In negative ion mode, charge compensation was achieved by applying low-energy electrons (5 eV) from a pulsed flood gun. All spectra were acquired with a primary ion dose $<10^{12}$ cm^{-2}.

Results and Discussion

The cyclic voltammogram obtained for the oxidation and reduction of a $FcC_{12}S$−Au monolayer on the cantilever chip (Figure 1) resembles those previously published for $FcC_{11}S$−Au.[40−42] Given the relative $FcC_{12}S$−Au-covered surface areas of the cantilevers ($\sim10^{-4}$ cm^2) and chip ($\sim$0.02−0.03 cm^2) immersed in the electrolyte solution, it is evident that the measured electrochemical current arises mainly from the chip substrate. An anodic peak at +0.33 V and a cathodic peak at +0.32 V correspond to the oxidation and reduction of the terminal ferrocenyl group, respectively. The small ($\sim$10 mV) separation between the anodic and cathodic peak potentials is consistent with the electrochemical transformation of an immobilized redox couple.[43] A shoulder is also observed on the negative side of each peak (at $\sim$+0.25 V and $\sim$+0.27 V). These multiple voltammetric waves are attributable to the presence of electrochemically distinct ferrocene environments.[44−47] A mean ferrocene surface coverage of 2.7(±0.3) × 10^{14} molecules/cm^2 was determined from the anodic peak area (44 ± 5 μC/cm^2). This gives an estimate of $\sim4 \times 10^{10}$ ferrocene groups on the actual cantilever surface. A TOF−SIMS ion map (Figure 1 inset) of Fe^+ (*m*/*z* ratio of 56 amu) confirmed the presence of the ferrocenyl species on the cantilever itself; no iron was detected on cantilevers modified with *n*-alkanethiols. TOF−SIMS analysis of the silicon nitride backside of an unmodified Au-coated cantilever chip showed the presence of some Au ($\sim$3% of a monolayer) on the cantilever legs (due to either the incomplete removal of the original Au coating with aqua regia or Au diffusion during thermal evaporation), but not on the chip substrate (Figures 2S and 3S).[48] The presence of this Au on the cantilever backside (high electrical resistance) is not expected to have a significant effect on the redox-induced surface stress changes described below.

An ellipsometric film thickness of 21.4 ± 1.5 Å was obtained in air for $FcC_{12}S$−Au monolayers prepared on macroscopic Au surfaces under the same conditions as the cantilevers. This value is in good agreement with that expected from the thickness of a $CH_3(CH_2)_{11}S$−Au monolayer (15 Å)[49,50] and the diameter of a ferrocenyl group (6.6 Å).[51] The film thickness and ferrocene surface coverage are consistent with a close-packed monolayer structure.[27,42,51,52]

Figure 2A,B presents typical current and deflection responses obtained for $FcC_{12}SH$-functionalized cantilevers during multiple cyclic voltammetric scans between 0 and +0.75 V. The anodic peak current decreases by $\sim$12% between the first and fourth cyclic voltammetric scan (Figure 2A) due to the well-documented decomposition of ferrocenium ions in the presence of even mild nucleophiles such as ClO_4^-.[15,53] The cantilever is deflected to a lower PSD voltage upon oxidation of the ferrocene (neutral form) to ferrocenium (cationic form) and returns to nearly its initial position when the ferrocenium is reduced back to ferrocene, although some drift is observed with time (Figure

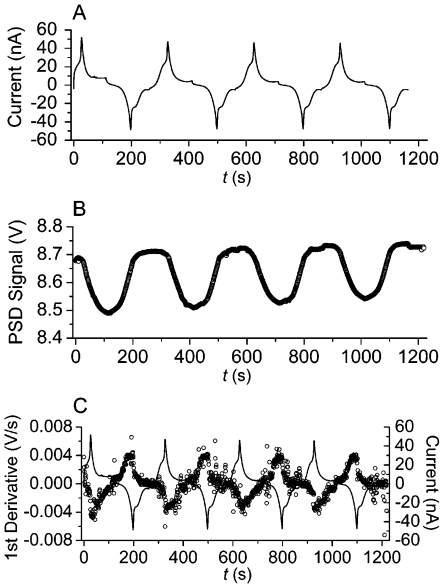

Figure 2. (A) Current vs time profile obtained during potential cycling between 0 and +0.75 V of a $FcC_{12}SH$-modified cantilever at a rate of 5 mV/s. Potential cycling was initiated at +0.19 V (open circuit potential). The supporting electrolyte is 1.0 M $HClO_4$. (B) Cantilever deflection (expressed as the PSD voltage) recorded during the potential cycles shown in A. (C) Plots of the current response (solid line) and first derivative of the cantilever deflection (circles) vs time.

2B). This drift only shifts the PSD signal-potential curves vertically with respect to each other without changing the relative cantilever response at a given potential value for a given redox cycle. Deflections to lower PSD voltages correspond to the cantilever bending away from its $FcC_{12}S-Au$ surface, and indicate that the electrochemical generation of the ferrocenium species generates a compressive interfacial stress change. Figure 2B shows that the magnitude of the cantilever deflection remains almost constant at ~0.2 V upon repeated cycling between the ferrocene and ferrocenium forms. Moreover, the first derivative plot of the deflection signal (Figure 2C) reveals that the maximum change in the cantilever motion occurs after the maximum anodic peak current is reached for ferrocene oxidation and before the maximum cathodic peak current is attained for ferrocenium reduction.

A comparison of the variation with the applied potential of the % change in cantilever deflection and the fractional surface coverage of ferrocenium (θ) is given in Figure 3. Such a comparison leads to the following significant observations. First, both curves (θ and % cantilever deflection) exhibit a sigmoidal shape. The % change in cantilever deflection attains a limiting value (defined as 100%) at $\theta = 1$ (i.e., all the ferrocene has been converted to ferrocenium) for the anodic scan (Figure 3A) and exhibits a constant value of 0% as θ approaches 0 in the cathodic scan (Figure 3B). This observation, and the fact that no appreciable change in the deflection signal is observed on cycling an electrochemically inert $C_{10}S-Au$ coated cantilever over the same potential range (Figure 4S), establish that the $FcC_{12}S-Au$ cantilever deflection is the result of the redox transformation of the ferrocenyl group. Second, bending of the cantilever is detectable (Figure 3A) only after ~15−20% conversion of the ferrocene into ferrocenium ($\theta \approx 0.15-0.2$). The cantilever reaches 50% of its maximum deflection at $\theta \approx 0.85-0.9$ (range obtained from measurements on several different cantilevers). During the cathodic scan, the PSD signal begins to change before there is any detectable reduction of the ferrocenium form (Figure 3B), and at 50% conversion ($\theta =$

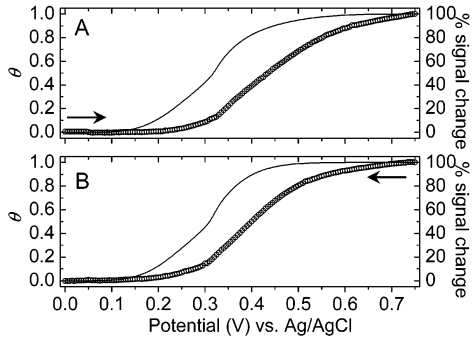

Figure 3. Plots of the fractional coverage (θ) of ferrocenium (solid lines) and % change in the cantilever deflection (circles) vs the applied potential: (A) anodic scan and (B) cathodic scan. θ was determined by integrating incrementally the areas under the anodic and cathodic current−potential curves of the cyclic voltammogram, after correction for the charging current by a baseline approximation. The % change in cantilever deflection was calculated by assigning the PSD signals at 0 V and +0.75 V to the zero cantilever position and the maximum cantilever deflection, respectively. The arrows indicate the direction of potential cycling.

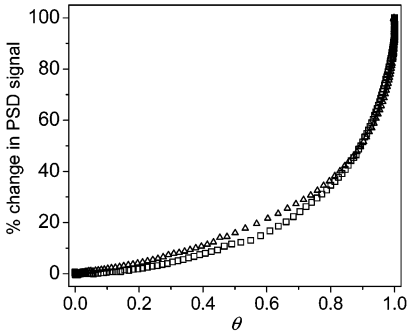

Figure 4. Plots of the % change in the cantilever deflection vs the fractional coverage of ferrocenium (θ) for anodic (squares) and cathodic (triangles) scans.

0.5), the $FcC_{12}S-Au$ cantilever has returned to within ~15−30% of its initial position. This behavior confirms the results shown in Figure 2C and has been repeatedly observed for all of the cantilevers investigated. A detailed summary of the relationship between the % change in cantilever deflection and θ is given in Figure 4 for the oxidation and reduction processes.

The polyaniline-coated cantilever system reported by Lahav et al.[26] is only superficially akin to the $FcC_{12}S-Au$ cantilevers used in the present study. A many-fold greater quantity of charge per cm^2 is generated during oxidation of the polyaniline film (cf. $FcC_{12}S-Au$ monolayer).[54] Stress changes arise from a combination of electrostatic and swelling effects in the polyaniline case.[26,55] On the other hand, stress changes in the SAM system studied here are attributable to electrostatic effects (see below), as close-packed $FcC_{12}S-Au$ monolayer films do not exhibit solvent incorporation/swelling phenomena.[27,40,52]

Origin of Surface Stress Change. The origins of the surface stress changes recorded in microcantilever experiments are often difficult to discern. For this reason, each likely source of the stress change observed here will be discussed in turn. A brief overview of what is known from different techniques on the processes that accompany electron transfer in ferrocenylalkanethiolate monolayers helps to place the results presented above into context. Cyclic voltammetry[41,44,45,56] and electrochemical quartz crystal microbalance (EQCM)[52] measurements have firmly established that the oxidation of surface-bound ferrocene is accompanied by a strong association of ClO_4^- with the electrogenerated ferrocenium to form a 1:1 ion pair at the

monolayer/solution interface. There is apparently no solvent uptake or ion penetration into close-packed ferrocenylalkanethiolate monolayers during oxidation.[52] The formation of ferrocenium cations and their association with ClO_4^- anions result in changes in the wetting properties of the monolayer. Contact angle[17,18] and adhesion force[15] measurements have shown that $FcCO_2C_{11}S-Au$ and $FcCOC_{15}S-Au$ surfaces are more hydrophilic after ferrocene oxidation, presumably due to the more polar character of the ferrocenium species (cf. neutral ferrocene).[17] Film structural changes have also been reported. In situ ellipsometry of $FcC_{11}S-Au$ demonstrated that oxidation of the terminal ferrocene moieties results in a 3 Å increase in the film thickness.[40] This increase in the film thickness was interpreted as resulting from both ferrocenium$-ClO_4^-$ ion-pair formation and a change in orientation of the ferrocenium group (with respect to neutral ferrocene), due to the smaller magnitude of the observed film thickness change compared to the ionic size of ClO_4^- (4.72 Å).[40,46] Subsequent in situ Fourier transform infrared reflection absorption spectroscopy (FT-IRRAS) measurements confirmed a redox-induced structural change.[27,42] The alkyl chains and ferrocene rings adopt a more perpendicular orientation upon ferrocene oxidation.[27,42]

Bearing this portrait in mind, the origin of the surface stress change shown in Figures 2B and 3 can now be addressed. To begin with, the most obvious origin of the surface stress change (i.e., interfacial properties) is not in fact operative. On the basis of the attractive ferrocenium$-ClO_4^-$ interaction and the decrease in the interfacial surface tension (monolayer/water), a *tensile* surface stress, corresponding to bending of the cantilever toward the film-coated Au side, would intuitively be expected to occur upon ferrocene oxidation in aqueous electrolyte solution. We have instead observed a compressive surface stress.[57] No potential dependent change in the double-layer structure of a $FcCO_2C_{11}S-Au$/solution interface was detected in force curves acquired by AFM,[15] and so double layer effects can be excluded. Other phenomena must therefore give rise to the observed compressive stress.

We presently consider film structural changes. Ye et al.[27,42] attribute the chain untilting transition observed by FT-IRRAS in close-packed $FcC_{11}S-Au$ monolayers to repulsive electrostatic interactions between the positively charged Au surface and the terminal ferrocenium cations. This rationale for the surface stress change is unlikely given that the positive ferrocenium charge is fully compensated by ClO_4^- anions.[18,41,44,45,52,56] We propose an alternative origin where the monolayer packing stress results from repulsive dipolar interactions between the ferrocenium-bearing alkanethiolates.[31,58] The apparent dipole moment of an alkanethiolate-Au monolayer is composed of contributions from $Au^{\delta+}-S^{\delta-}$ and from $S^{\delta-}-R^{\delta+}$,[59,60] where the partial charge on the S determined by X-ray photoelectron spectroscopy[61] is $\sim 0.2e$. Formation of the ferrocenium$-ClO_4^-$ ion pair at the monolayer/electrolyte interface should increase the apparent molecular dipole moment and the magnitude of the associated dipolar repulsive forces between the alkanethiolate molecules. Such dipolar repulsive forces have already been identified as being the source of the compressive surface stress changes observed during the self-assembly of *n*-alkanethiols on Au-coated microcantilevers.[31,58] The ferrocenium-bearing alkyl chains can untilt, as suggested by FT-IRRAS,[27,42] to relieve these repulsive electrostatic interactions (due to increased chain-chain separation). Both phenomena (repulsive dipolar forces and alkyl chain untilting) would result in an expanding lateral tension which could drive the cantilever deflection reported herein.[31,58]

Dynamics of Surface Stress Change. Although the cantilever response time is fast ($\sim$1 ms)[23] and the potential scan rate is slow (5 mV/s), the $FcC_{12}S-Au$ cantilever begins to deflect only after $\sim$20% conversion of the ferrocene into ferrocenium ($\theta \approx 0.2$) and is at 50% of its maximum deflection at $\sim$90% conversion ($\theta \approx 0.9$). Moreover, on the reductive scan, the cantilever returns back to within $\sim$15$-$30% of its initial position at 50% conversion of ferrocenium to ferrocene ($\theta = 0.5$). This is probably due to the fact that the current response reflects individual electron transfer events, whereas the cantilever reports an ensemble of events. Although ion-pairing occurs simultaneously with electron transfer,[52,62] the associated monolayer restructuring[27,42] can be expected to occur on a different time scale. This can explain why although the fractional ferrocenium coverage and % cantilever deflection vs potential curves are both sigmoidal in shape, they are offset from each other (Figure 3). Such behavior has been observed for other ferrocenylalkanethiolate monolayer properties at a potential scan rate (10 mV/s) comparable to the one used here. For instance, the $FcC_{11}S-Au$ film thickness begins to change with ferrocene oxidation but continues at potentials higher than the current-peak potential.[40] Sondag-Huethorst and Fokkink found that the contact angle of an $FcCO_2C_{11}S-Au$ monolayer starts to change after more than 50% of the ferrocene (or ferrocenium) groups have been oxidized (or reduced).[18] Finally, it is clear that the monolayer structure/state being ostensibly different at the beginning and end of an oxidative cycle,[27,40,42] the cantilever response dynamics during the subsequent reductive scan are not expected to mirror that of the preceding anodic scan (Figure 3).

Potential step experiments (from a non-oxidizing to an oxidizing potential) and cyclic voltammetry performed at different scan rates will serve to establish the dynamics of the surface stress change. Quantifying the stress change (in N/m) associated with the measured cantilever deflection[23,38,39,63] may also help to consolidate the proposed cantilever actuation mechanism.

Conclusion

We have shown that the electrochemical oxidation/reduction of $\sim 4 \times 10^{10}$ ferrocene groups positioned $\sim$21 Å away from the metal-coated cantilever surface exerts a force of sufficient magnitude to induce cantilever motion. We attribute the potential-induced bending of a $FcC_{12}S-Au$ coated cantilever to electrostatic forces and structural changes occurring in the ferrocenyldodecanethiolate monolayer due to the electrochemical generation of ferrocenium cations. The significance of this work is that it demonstrates that ultrathin electroactive monolayer films of well-defined structure can be used for micromechanical actuation. Although most studies involving electroactive SAMs have until now largely focused on the interfacial electron-transfer kinetics, surface stress measurements using AFM cantilevers may provide new insights into the physical and chemical processes which accompany redox reactions at modified electrodes.

Acknowledgment. We thank Suzie Poulin (École Polytechnique de Montréal) for TOF-SIMS analysis, Oleh Tanchak (McGill University) for ellipsometry measurements, Brian Seivewright (McGill) and the cantilever sensor group of Prof. Peter Grütter (McGill) for sharing their technical knowledge. This work was supported by NSERC (Canada), Canada Foundation for Innovation (New Opportunities), and the Research Corporation (USA). F.Q. gratefully acknowledges fellow-

ship support from the Groupe de recherche en technologie des couches minces.

Supporting Information Available: Schematic of the electrochemical liquid cell (Figure 1S), TOF−SIMS Au^+ ion maps and spectra of cantilevers (Figures 2S and 3S), and potential-induced deflection response of a $C_{10}S$−Au cantilever (Figure 4S). This material is available free of charge via the Internet at http://pubs.acs.org.

References and Notes

(1) Butt, H.-J. *J. Colloid Interface Sci.* **1996**, *180*, 251−260.

(2) Thundat, T.; Oden, P. I.; Warmack, R. J. *Microscale Thermophys. Eng.* **1997**, *1*, 185−199.

(3) Moulin, A. M.; O'Shea, S. J.; Welland, M. E. *Ultramicroscopy* **2000**, *82*, 23−31.

(4) Raiteri, R.; Grattarola, M.; Butt, H.-J.; Skladal, P. *Sens. Actuators B* **2001**, *79*, 115−126.

(5) Lang, H. P.; Hegner, M.; Meyer, E.; Gerber, C. *Nanotechnology* **2002**, *13*, R29−R36.

(6) Sepaniak, M.; Datskos, P.; Lavrik, N.; Tipple, C. *Anal. Chem.* **2002**, *74*, 568A−575A.

(7) Fritz, J.; Baller, M. K.; Lang, H. P.; Strunz, T.; Meyer, E.; Güntherodt, H.-J.; Delamarche, E.; Gerber, C.; Gimzewski, J. K. *Langmuir* **2000**, *16*, 9694−9696.

(8) Raiteri, R.; Butt, H.-J.; Grattarola, M. *Electrochim. Acta* **2000**, *46*, 157−163.

(9) Ji, H.-F.; Hansen, K. M.; Hu, Z.; Thundat, T. *Sens. Actuators B* **2001**, *72*, 233−238.

(10) Xu, J.; Li, H.-L. *J. Colloid Interface Sci.* **1995**, *176*, 138−149.

(11) Gooding, J. J.; Mearns, F.; Yang, W.; Liu, J. *Electroanalysis* **2003**, *15*, 81−96 and references therein.

(12) Ulman, A. *Chem. Technol.* **1995**, 22−28.

(13) Chidsey, C. E. D. *Science* **1991**, *251*, 919−922.

(14) Smalley, J. F.; Finklea, H. O.; Chidsey, C. E. D.; Linford, M. R.; Creager, S. E.; Ferraris, J. P.; Chalfant, K.; Zawodzinski, T.; Feldberg, S. W.; Newton, M. D. *J. Am. Chem. Soc.* **2003**, *125*, 2004−2013 and references therein.

(15) Green, J.-B. D.; McDermott, M. T.; Porter, M. D. *J. Phys. Chem.* **1996**, *100*, 13342−13345.

(16) Hudson, J. E.; Abruña, H. D. *J. Am. Chem. Soc.* **1996**, *118*, 6303−6304.

(17) Abbott, N. L.; Whitesides, G. M. *Langmuir* **1994**, *10*, 1493−1497.

(18) Sondag-Huethorst, J. A. M.; Fokkink, L. G. J. *Langmuir* **1994**, *10*, 4380−4387.

(19) Ivanisevic, A.; Im, J.-H.; Lee, K.-B.; Park, S.-J.; Demers, L. M.; Watson, K. J.; Mirkin, C. A. *J. Am. Chem. Soc.* **2001**, *123*, 12424−12425.

(20) Díaz, D. J.; Hudson, J. E.; Storrier, G. D.; Abruña, H. D.; Sundararajan, N.; Ober, C. K. *Langmuir* **2001**, *17*, 5932−5938.

(21) Yousaf, M. N.; Mrksich, M. *J. Am. Chem. Soc.* **1999**, *121*, 4286−4287.

(22) Hodneland, C. D.; Mrksich, M. *J. Am. Chem. Soc.* **2000**, *122*, 4235−4236.

(23) Brunt, T. A.; Rayment, T.; O'Shea, S. J.; Welland, M. E. *Langmuir* **1996**, *12*, 5942−5946.

(24) Brunt, T. A.; Chabala, E. D.; Rayment, T.; O'Shea, S. J.; Welland, M. E. *J. Chem. Soc., Faraday Trans.* **1996**, *92*, 3807−3812.

(25) Raiteri, R.; Butt, H.-J. *J. Phys. Chem.* **1995**, *99*, 15728−15732.

(26) Lavah, M.; Durkan, C.; Gabai, R.; Katz, E.; Willner, I.; Welland, M. E. *Angew. Chem., Int. Ed.* **2001**, *40*, 4095−4097.

(27) Ye, S.; Haba, T.; Sato, Y.; Shimazu, K.; Uosaki, K. *Phys. Chem. Chem. Phys.* **1999**, *1*, 3653−3659.

(28) Creager, S. E.; Rowe, G. K. *J. Electroanal. Chem.* **1994**, *370*, 203−211.

(29) Hickman, J. J.; Ofer, D.; Zou, C.; Wrighton, M. S.; Laibinis, P. E.; Whitesides, G. M. *J. Am. Chem. Soc.* **1991**, *113*, 1128−1132.

(30) Laibinis, P. E.; Hickman, J. J.; Wrighton, M. S.; Whitesides, G. M. *Science* **1989**, *245*, 845−847.

(31) Berger, R.; Delamarche, E.; Lang, H. P.; Gerber, C.; Gimzewski, J. K.; Meyer, E.; Güntherodt, H.-J. *Science* **1997**, *276*, 2021−2024.

(32) Ratieri, R.; Nelles, G.; Butt, H.-J.; Knoll, W.; Skládal, P. *Sens. Actuators B* **1999**, *61*, 213−217.

(33) Ji, H.-F.; Finot, E.; Dabestani, R.; Thundat, T.; Brown, G. M.; Britt, P. F. *Chem. Commun.* **2000**, 457−458.

(34) Fritz, J.; Baller, M. K.; Lang, H. P.; Rothuizen, H.; Vettiger, P.; Meyer, E.; Güntherodt, H.-J.; Gerber, C.; Gimzewski, J. K. *Science* **2000**, *288*, 316−318.

(35) Wu, G.; Ji, H.; Hansen, K.; Thundat, T.; Datar, R.; Cote, R.; Hagan, M. F.; Chakraborty, A. K.; Majumdar, A. *Proc. Natl. Acad. Sci. U.S.A.* **2001**, *98*, 1560−1564.

(36) Wu, G.; Datar, R. H.; Hansen, K. M.; Thundat, T.; Cote, R. J.; Majumdar, A. *Nat. Biotechnol.* **2001**, *19*, 856−860.

(37) Arntz, Y.; Seelig, J. D.; Lang, H. P.; Zhang, J.; Hunziker, P.; Ramseyer, J. P.; Meyer, E.; Hegner, M.; Gerber, C. *Nanotechnology* **2003**, *14*, 86−90.

(38) Godin, M. M. Sc. thesis, Department of Physics, McGill University, Montreal, QC, Canada, 2000.

(39) Godin, M.; Tabard-Cossa, V.; Grütter, P. *Appl. Phys. Lett.* **2001**, *79*, 551−553.

(40) Ohtsuka, T.; Sato, Y.; Uosaki, K. *Langmuir* **1994**, *10*, 3658−3662.

(41) Uosaki, K.; Sato, Y.; Kita, H. *Langmuir* **1991**, *7*, 1510−1514.

(42) Ye, S.; Sato, Y.; Uosaki, K. *Langmuir* **1997**, *13*, 3157−3161.

(43) Bard, A. J.; Faulkner, L. R. *Electrochemical Methods Fundamentals and Applications*, 2nd ed.; J. Wiley & Sons: New York, 2001.

(44) Creager, S. E.; Rowe, G. K. *Anal. Chim. Acta* **1991**, *246*, 233−239.

(45) Rowe, G. K.; Creager, S. E. *Langmuir* **1991**, *7*, 2307−2312.

(46) Rowe, G. K.; Creager, S. E. *J. Phys. Chem.* **1994**, *98*, 5500−5507.

(47) Walczak, M. M.; Popenoe, D. D.; Deinhammer, R. S.; Lamp, B. D.; Chung, C.; Porter, M. D. *Langmuir* **1991**, *7*, 2687−2693.

(48) Lo, Y.-S.; Huefner, N. D.; Chan, W. S.; Dryden, P.; Hagenhoff, B.; Beebe, T. P., Jr. *Langmuir* **1999**, *15*, 6522−6526.

(49) Bain, C. D.; Troughton, E. B.; Tao, Y.-T.; Evall, J.; Whitesides, G. M.; Nuzzo, R. G. *J. Am. Chem. Soc.* **1989**, *111*, 321−335.

(50) Biebuyck, H. A.; Bain, C. D.; Whitesides, G. M. *Langmuir* **1994**, *10*, 1825−1831.

(51) Chidsey, C. E. D.; Bertozzi, C. R.; Putvinski, T. M.; Mujsce, A. M. *J. Am. Chem. Soc.* **1990**, *112*, 4301−4306.

(52) Shimazu, K.; Yagi, I.; Sato, Y.; Uosaki, K. *J. Electroanal. Chem.* **1994**, *372*, 117−124.

(53) Popenoe, D. D.; Deinhammer, R. S.; Porter, M. D. *Langmuir* **1992**, *8*, 2521−2530.

(54) On the basis of the polyaniline film thickness of 190 nm reported by Lavah et al., the relation between the anodic charge density and the film thickness (Guiseppi-Elie, A.; Pradhan, S. R.; et al. *Chem. Mater*. **1993**, *5*, 1474−1480) suggests that a ca. 300-fold greater quantity of charge per cm^2 is electrogenerated at the polyaniline-coated cantilever compared to the $FcC_{12}S$−Au cantilever.

(55) Chegel, V.; Raitman, O.; Katz, E.; Gabai, R.; Willner, I. *Chem. Commun.* **2001**, 883−884.

(56) Ju, H.; Leech, D. *Phys. Chem. Chem. Phys.* **1999**, *1*, 1549−1554.

(57) A tensile surface stress change has been reported for binding of CrO_4^{2-} ions to SAMs of Au−$S(CH_2)_{12}$−N−$(CH_2CH_3)_3^+Br^-$ (Ji, H.-F.; Thundat, T.; et al. *Anal. Chem*. **2001**, *73*, 1572−1576). This contracting surface stress change is due to the replacement of a surface-confined 1:1 quaternary ammonium:Br^- ion pair by a 2:1 quaternary ammonium:CrO_4^{2-} ion pair.

(58) Berger, R.; Delamarche, E.; Lang, H. P.; Gerber, C.; Gimzewski, J. K.; Meyer, E.; Güntherodt, H.-J. *Appl. Phys. A* **1998**, *66*, S55−S59.

(59) Evans, S. D.; Ulman, A. *Chem. Phys. Lett.* **1990**, *170*, 462−466.

(60) Boubour, E. Ph.D. Thesis, Department of Chemistry, McGill University, Montreal, QC, Canada, 2000.

(61) Bourg, M.-C.; Badia, A.; Lennox, R. B. *J. Phys. Chem. B* **2000**, *104*, 6562−6567.

(62) Sumner, J. J.; Creager, S. E. *J. Phys. Chem. B* **2001**, *105*, 8739−8745.

(63) O'Shea, S. J.; Welland, M. E.; Brunt, T. A.; Ramadan, A. R.; Rayment, T. *J. Vac. Sci. Technol. B* **1996**, *14*, 1383−1385.